Science Advances
AAAS

Supplementary Materials for

The earliest basketry in southern Europe: Hunter-gatherer and farmer plant-based technology in Cueva de los Murciélagos (Albuñol)

Francisco Martínez-Sevilla *et al.*

Corresponding author: Francisco Martínez-Sevilla, f.martinezs@uah.es

Sci. Adv. **9**, eadi3055 (2023)
DOI: 10.1126/sciadv.adi3055

This PDF file includes:

Supplementary Text

Site location

The cave is located on the south face of the Sierra de la Contraviesa in La Unidad de Lujar-Gádor (Albuñol tectonic window). This is the lower unit of the Alpujárride Complex and comprises, from bottom to top, of limestone marble, tabled marble of the middle and upper Triassic ages, and a gap of Neogene age. Above this unit sit the Alcázar Unit, the Murtas Unit and the Adra Unit, all of them composed of schists, calcoschists, limestone and phyllite. Together with the Sierra de Lujar and the Sierra de Gádor, the Sierra de La Contraviesa constitutes a W-E tectonic alignment between Sierra Nevada to the north and the Mediterranean Sea to the south, separated by the Guadalfeo river valley. This tectonic alignment on the edge of the Mediterranean belongs to the Alpujárride Complex of the Betic Cordillera. As a consequence of the slope and the Mediterranean climate, the hydrological network is remarkably embedded, generating gorges such as the Barranco de las Angosturas (about 100 m deep), which drains from north to south, flowing into the Mediterranean.

Radiocarbon dated objects

475: The mallet was made from a single piece of olive wood (*Olea europaea)* (Fig. 6A). The head of the mallet is double-faced and was made with part of the trunk. It was shaped by cutting and splitting the trunk; the tool-marks are still visible in the surface of the wood. Four knots are visible in the surface of the mallet head. This part is 142 mm long, 44.94 mm maximum wide and 36.00 mm high. The handle was formed by the branch growing out from the stem. The proximal part of the handle is cracked and partially broken. The preserved length of the object, including the handle and the head, is 283 mm. The maximum diameter of the distal part of handle is 38.00 mm, and in the middle, it measures 19.00mm; the proximal part was not measured because it does not preserve the original morphology. The functional classification as mallet is based on morphology and on the wear marks on the edges of the double-head, where the wood fibers were clearly crushed by repetitive pounding. The surface also preserves polished areas, probably related to hand friction during use.

479: The pointed object was made from a twig of strawberry tree (*Arbutus unedo*) (Fig. 5C). The twig preserves four knots indicating that lateral sprouts were cut from these places. It is 239 mm long and the maximum diameter in the proximal part is 14.96 mm. The distal part of the object preserves tool marks related to the shaping of the active edge. Crushed wood fibers and polished surfaces are visible on the pointed edge, indicating that this was the active part of the tool.

579: Small close simple twining with S-twist wefts basket, completely conserved (Fig. 4A). It has a cylindrical form and tapers slightly at the top (or the neck). It measures approximately 90 mm in diameter at the top and 130 mm in height, the interior volume is 711 cm^3. The basket is started with a bunch of fibers which is divided into 12 parts. After five rows these are divided again to increase the size of the basket. The warp starts with more than two leaves of esparto, but when the base of the basket is complete, it is made by at least two leaves. Otherwise, the weft consists of four esparto leaves (two in each strand) on the base of the object, but the walls are made with a single leave in each strand. The basket is finished at the top, where the fibers are wrapped and knotted, forming a cylinder along the upper edge. Two handles are present on the top of the basket, both on one side and separated by 67 mm. These consist of two circular perforations (each 3 mm

in diameter) reinforced by 60 mm of animal skin that covers the perforation from inside to outside and wraps the rim. These are sewed in a V-shaped with three to four stitches on a single esparto leaf. Newly added fibers are visible inside the basket. The object presents decorations made by dyed esparto leaves forming geometric figures all around the basket, and these are different to the fibers forming the rim and the rest of the basket. Raw material seems to be narrow, raw leaves of esparto.

580: Small close simple twining with S-twist wefts basket, nearly complete, except for the upper margin, almost half of which is absent (Fig. 4B). The rim was sewn as part of by conservation processes in the museum. The basket, which is 100 mm in height, is cylindrical and slightly narrower at the top. Its upper opening is oval in shape (probably distorted) and measures about 50x65 mm, the interior volume is 329,6 cm^3. The construction starts with a bunch of several fibers divided into 14 parts; after four or five rows, they are divided again to make the base wider. This means that the warp starts with more than three leaves of esparto, but when the base of the basket is done, they are made by less than three leaves. In this case, the wefts are always made by a single esparto leaf in each strand, both for the base and the walls. The rim of the basket is wrapped and sewn in several places. Newly added fibers are visible inside the basket. Decoration is just visible in the form of vertical and horizontal lines created by the use of differently dyed fibers. The raw material seems to be narrow, raw leaves of esparto.

581: Small close simple twining with S-twist wefts basket. It is cylindric-shaped but is slightly wider at the base (Fig. 4C). It measures 58 mm in diameter at the top and is 97 mm in height, the interior volume is 267,4 cm^3. The basket is constructed by first crossing two small bundles, each probably comprising four leaves. These bundles are initially wrapped together, and then separated after four, and then after eight rows, to increase the volume and form the shape of the basket. Both warp and weft are formed from a single leaf of esparto. The basket is finished by wrapping and knotting the fibers. The addition of fibers is visible inside the basket. Decoration made from dyed fibers are present across the body of the basket; different patterns are located on the neck and the rest of the object. The fibers used are narrow, raw leaves of esparto.

594: Bag made with the *cofín* basketry technique (Fig. 5B). The object is constructed from a braided ring, with new fibers added to make it wider. The body of the bag is formed from spaced braids (5-15 mm), which makes it possible to see through the basket, or to see the contents. It is made of 11 rows and finished at the top with a new closed braid which wraps all the fibers from the previous braids. Each strand is made of two raw esparto leaves. The bag has a handle, 7 mm in width, which consists of a braid knotted to the rim.

598: Fragmented central core type sandal (Fig. 7B), although most of the bundles that surround the central core are missing because of radiocarbon sampling in the nineties (38). The conserved fragment is 150 mm long. A single bundle is conserved on the rear part, while in the front part a single bundle is partially present. A braided crossing of the central core is visible. The fibers appear slightly crushed.

603: Complete central core type sandal - slightly distorted (Fig. 6B). The sandal measures 190 mm long, and is 71 mm wide at the front and 58 mm wide at the back. It is composed of central core, 132 mm in length. The front part is made of three bundles, while the rear part is composed of two

bundles, making the front of the sandal wider. Two braids are visible on the upper face of the sandal, likely used to tie the shoe to the feet. No pressure deformities are visible on the upper face, and no use wear is present on the lower part. Moreover, the basal part of the esparto leaves is still present, suggesting the sandal might be unfinished or not used. The esparto used to produce this object was partially crushed.

609: Fragmented central core type sandal (Fig. 7C). Important parts of the object are missing because it was used in the previous ^{14}C dating analyses (38). fresh cuts are visible in some of the bundles. The conserved fragment is 165 mm long. Although two bundles are missing in the front part, it measures 65 mm wide; one bundle is missing from the rear part, which measures 50 mm wide. Knotted braids for tying the shoe to the foot are conserved. Sediment is attached to the upper part of the sole, and the lower face presents use-wear. The fibers appear slightly crushed.

611: Simple type sandal which is fragmented (Fig. 6C). The sole is almost complete but the front part is absent. The length of the conserved fragment is about 183 mm, the width of the back part is 65 mm and front part is 100 mm wide. The sandal is composed of a braid wrapped five times around itself, increasing the width of the sandal sole. Braids for tying the shoe to the foot originate from the middle edges of the sole, along with a knot near the back part, but no further details can be described. A clear pressure deformity is visible on the back of the upper face. The lower part has attached sediment and the fibers show signs of use. The fibers appear partially crushed.

615: Large fragment made by close coiling (Fig. 8C). No curvature is visible so the object could be part of a large basket or a rectangular mat. Its preservation is good, although it is a fragment and no edges are present. It measures 390 mm long, 270 mm wide, and 4-5 mm is thick. The active element is composed of a single leaf which is stitched twice in the same place. One face is not visible because it is attached to an exposing surface. The esparto appears slightly crushed.

616a: There are currently two registers in the museum designated 616 (616a and 616b). They were probably part of the same object, but by comparing the images published by Alfaro (29, 30), we can determine that the fragment used for radiocarbon studies in the nineties was 616a (Fig. 7A) (38). This piece shows a fresh cutting area where the sample was extracted for these studies. The object is a fragment of a basket made by close coiling (230 mm long, 8 mm wide, 5.8 mm thick). The foundation is composed of 6 or 7 leaves of esparto and it is 4.5-4.9 mm thick. The active element is composed of a single leaf which is stitched twice in the same place. It shows V-shaped stitches on the outer face. The esparto seems to be slightly crushed.

617: Fragment made with close simple twining with S-twist wefts basketry technique (Fig. 5A). Although being a fragment, it has a good state of preservation. It measures 270 mm in length and 140 mm in width. The weft is formed from two leaves of esparto, each strand being 6.2-6.6 mm long and 3.4-3.6 mm wide). The warp is formed from 4 to 5 leaves, but this varies along the fragment in order to maintain a homogeneous thickness (2.3-2.8 mm). A change in the twist of the weft from S- to Z-twist is visible as a decorative row in the middle of the fragment.

623: Large fragment made by the *cofín* basketry technique (370 mm x 240 mm) (Fig. 8A). The object presents a space of 7-14 mm between rows. It preserves the rim which is a wide braid, wrapping the fibers from the body of the object. A hole is present in the middle of the object. Each strand is made by 5 or 6 crushed leaves of esparto, the number of fibers varying along the fragment

to maintain homogeneous thickness. An independent braid is attached to the object; this could be part of a handle.

624: Fragment made with the *cofín* basketry technique, but avowing variations in the spacing between the rows (Fig. 8D). In the central section, the object presents a closed-*cofín* braiding (diameter of 51 mm), then a 2 mm spaced-*cofín* braiding (150 mm) and, finally, a closed-*cofín* braiding (33 mm). In this last section, it appears that three rows, each made using different stitches, create three decorative lines. The central and initial braids are longer than those in the rest of the object. The rim is fragmented so more details can be described. Each strand is made of a single, slightly crushed esparto leaf.

625: Bag started with five knots on the base, which form the warp (Fig. 8B). A braid is started and is crossed by the warp which holds the knots together to form a circle. For each row the width is increased by adding more braids to the inside with the warp. After five rows, the braid warps and the bag are finished with a thicker braid on the rim. As the warp crosses the horizontal element (the braid), this is movable up and down. Two leaves of raw esparto are used in each strand of the braid. A braided handle is attached to the last row (which form the rim). Raw esparto is used.

626: Four rings formed from a twisted bundle of fibers and wrapped with an opened leaf of esparto (Fig. 4D). The rings are currently open, but they could originally have been linked. They are approximately 7 mm wide. The esparto leaves appear to be raw.

OxCal code for Bayesian analyses used in this study

1. Oxcal SQL code

1.1. KDE models

1.1.1. KDE_plot two phases

```
Plot()
 {
  Sequence(Los Murciélagos)
  {
   Boundary("Start")
   {
    color="green";
   };
   Phase()
   {
    KDE_Plot("")
    {
    };
    R_Date("Beta-627332", 8350, 30);
    R_Date("Beta-627333", 8320, 30);
    R_Date("Beta-627334", 8300, 30);
    R_Date("CSIC-247", 7440, 100);
```

```
   R_Date("Beta-627342", 6210, 30);
   R_Date("Beta-627340", 6170, 30);
   R_Date("Beta-628427", 6150, 30);
   R_Date("CSIC-1133", 6086, 45);
   R_Date("CSIC-1134", 5900, 38);
   R_Date("CSIC-1132", 5861, 48);
   R_Date("Beta-627338", 5660, 30);
   R_Date("Beta-627331", 5640, 30);
   R_Date("Beta-627330", 5630, 30);
   R_Date("Beta-627341", 5580, 30);
   R_Date("Beta-627337", 5570, 30);
   R_Date("Beta-627336", 5550, 30);
   R_Date("Beta-627335", 5550, 30);
   R_Date("CSIC-246", 5400, 80);
   R_Date("CSIC-247", 7440, 100);
  };
  Boundary("End ")
  {
   color="red";
  };
 };
};
Plot()
{
 Sequence("Phase 1")
 {
  Boundary("Start")
  {
   color="grey";
  };
  Phase()
  {
   KDE_Plot("Plot")
   {
   };
   R_Date("Beta-628426", 8400, 30);
   R_Date("Beta-627332", 8350, 30);
   R_Date("Beta-627333", 8320, 30);
   R_Date("Beta-627334", 8300, 30);
  };
  Boundary("End ")
  {
   color="blue";
  };
 };
};
```

```
Plot()
{
 Sequence("Phase 2")
 {
  Boundary("Start")
  {
   color="yellow";
  };
  Phase()
  {
   KDE_Plot("Plot")
   {
   };
   R_Date("Beta-627342", 6210, 30);
   R_Date("Beta-627340", 6170, 30);
   R_Date("Beta-628427", 6150, 30);
   R_Date("CSIC-1133", 6086, 45);
   R_Date("CSIC-1134", 5900, 38);
   R_Date("CSIC-1132", 5861, 48);
   R_Date("Beta-627338", 5660, 30);
   R_Date("Beta-627331", 5640, 30);
   R_Date("Beta-627330", 5630, 30);
   R_Date("Beta-627341", 5580, 30);
   R_Date("Beta-627337", 5570, 30);
   R_Date("Beta-627336", 5550, 30);
   R_Date("Beta-627335", 5550, 30);
   R_Date("CSIC-246", 5400, 80);
  };
  Boundary("End ")
  {
   color="purple";
  };
 };
};
```

1.1.3. KDE_plot three phases

```
Plot()
 {
  Sequence("Los Murciélagos")
  {
   Boundary()
   {
    color="green";
   };
   Phase()
```

```
  {
   KDE_Plot("Los Murciélagos")
   {
   };
   R_Date("Beta-627332", 8350, 30);
   R_Date("Beta-627333", 8320, 30);
   R_Date("Beta-627334", 8300, 30);
   R_Date("CSIC-247", 7440, 100);
   R_Date("Beta-627342", 6210, 30);
   R_Date("Beta-627340", 6170, 30);
   R_Date("Beta-628427", 6150, 30);
   R_Date("CSIC-1133", 6086, 45);
   R_Date("CSIC-1134", 5900, 38);
   R_Date("CSIC-1132", 5861, 48);
   R_Date("Beta-627338", 5660, 30);
   R_Date("Beta-627331", 5640, 30);
   R_Date("Beta-627330", 5630, 30);
   R_Date("Beta-627341", 5580, 30);
   R_Date("Beta-627337", 5570, 30);
   R_Date("Beta-627336", 5550, 30);
   R_Date("Beta-627335", 5550, 30);
   R_Date("CSIC-246", 5400, 80);
  };
  Boundary()
  {
   color="red";
  };
 };
};
Plot()
{
 Sequence("Phase 1")
 {
  Boundary()
  {
   color="green";
  };
  Phase()
  {
   KDE_Plot("Phase 1")
   {
   };
   R_Date("Beta-628426", 8400, 30);
   R_Date("Beta-627332", 8350, 30);
   R_Date("Beta-627333", 8320, 30);
   R_Date("Beta-627334", 8300, 30);
```

```
   };
   Boundary()
   {
    color="red";
   };
  };
 };
Plot()
 {
  Sequence("Phase 2")
  {
   Boundary()
   {
    color="green";
   };
   Phase()
   {
    KDE_Plot("Phase 2")
    {
    };
    R_Date("CSIC-247", 7440, 100);
   };
   Boundary()
   {
    color="red";
   };
  };
 };
 Plot()
 {
  Sequence("Phase 3")
  {
   Boundary()
   {
    color="green";
   };
   Phase()
   {
    KDE_Plot("Phase 3")
    {
    };
    R_Date("Beta-627342", 6210, 30);
    R_Date("Beta-627340", 6170, 30);
    R_Date("Beta-628427", 6150, 30);
    R_Date("CSIC-1133", 6086, 45);
    R_Date("CSIC-1134", 5900, 38);
```

```
    R_Date("CSIC-1132", 5861, 48);
    R_Date("Beta-627338", 5660, 30);
    R_Date("Beta-627331", 5640, 30);
    R_Date("Beta-627330", 5630, 30);
    R_Date("Beta-627341", 5580, 30);
    R_Date("Beta-627337", 5570, 30);
    R_Date("Beta-627336", 5550, 30);
    R_Date("Beta-627335", 5550, 30);
    R_Date("CSIC-246", 5400, 80);
   };
   Boundary()
   {
    color="red";
   };
  };
 };
```

1.2. Bayesian models

1.2.1. Single phase model

```
Plot()
 {
  Sequence("Los Murciélagos")
  {
   Boundary("Start Los Murciélagos")
   {
    color="green";
   };
   Phase("Los Murciélagos")
   {
    R_Date("Beta-628426", 8400, 30);
    R_Date("Beta-627332", 8350, 30);
    R_Date("Beta-627333", 8320, 30);
    R_Date("Beta-627334", 8300, 30);
    R_Date("CSIC-247", 7440, 100);
    R_Date("Beta-627342", 6210, 30);
    R_Date("Beta-627340", 6170, 30);
    R_Date("Beta-628427", 6150, 30);
    R_Date("CSIC-1133", 6086, 45);
    R_Date("CSIC-1134", 5900, 38);
    R_Date("CSIC-1132", 5861, 48);
    R_Date("Beta-627338", 5660, 30);
    R_Date("Beta-627331", 5640, 30);
    R_Date("Beta-627330", 5630, 30);
    R_Date("Beta-627341", 5580, 30);
```

```
   R_Date("Beta-627337", 5570, 30);
   R_Date("Beta-627336", 5550, 30);
   R_Date("Beta-627335", 5550, 30);
   R_Date("CSIC-246", 5400, 80);
   Interval ("Los Murciélagos");
  };
  Boundary("End Los Murciélagos")
  {
   color="red";
  };
 };
};
```

1.2.2. Multi-phase model_two phases

```
Plot()
 {
  Sequence("Los Murciélagos")
  {
   Boundary("Start 1")
   {
    color="green";
   };
   Phase("1")
   {
    R_Date("Beta-628426", 8400, 30);
    R_Date("Beta-627332", 8350, 30);
    R_Date("Beta-627333", 8320, 30);
    R_Date("Beta-627334", 8300, 30);
    Interval("1");
   };
   Boundary("End 1")
   {
    color="red";
   };
   Boundary("Start 2")
   {
    color="green";
   };
   Phase("2")
   {
    R_Date("Beta-627342", 6210, 30);
    R_Date("Beta-627340", 6170, 30);
    R_Date("Beta-628427", 6150, 30);
    R_Date("CSIC-1133", 6086, 45);
    R_Date("CSIC-1134", 5900, 38);
```

```
   R_Date("CSIC-1132", 5861, 48);
   R_Date("Beta-627338", 5660, 30);
   R_Date("Beta-627331", 5640, 30);
   R_Date("Beta-627330", 5630, 30);
   R_Date("Beta-627341", 5580, 30);
   R_Date("Beta-627337", 5570, 30);
   R_Date("Beta-627336", 5550, 30);
   R_Date("Beta-627335", 5550, 30);
   R_Date("CSIC-246", 5400, 80);
   Interval("2");
  };
  Boundary("End 2")
  {
   color="red";
  };
 Difference("Difference Phase 1 to Phase 2", "End 1", "Start 2");
 };
};
```

1.2.3. Multi-phase model three phases

```
Plot()
 {
  Sequence("Los Murciélagos")
  {
   Boundary("Start 1")
   {
    color="green";
   };
   Phase("1")
   {
    R_Date("Beta-628426", 8400, 30);
    R_Date("Beta-627332", 8350, 30);
    R_Date("Beta-627333", 8320, 30);
    R_Date("Beta-627334", 8300, 30);
    Interval("1");
   };
   Boundary("End 1")
   {
    color="red";
   };
   Boundary("Start 2")
   {
    color="green";
   };
```

```
  Phase("2")
  {
   R_Date("CSIC-247", 7440, 100);
   Interval("2");
  };
  Boundary("End 2")
  {
   color="red";
  };
  Boundary("Start 3")
  {
   color="green";
  };
  Phase("3")
  {
   R_Date("Beta-627342", 6210, 30);
   R_Date("Beta-627340", 6170, 30);
   R_Date("Beta-628427", 6150, 30);
   R_Date("CSIC-1133", 6086, 45);
   R_Date("CSIC-1134", 5900, 38);
   R_Date("CSIC-1132", 5861, 48);
   R_Date("Beta-627338", 5660, 30);
   R_Date("Beta-627331", 5640, 30);
   R_Date("Beta-627330", 5630, 30);
   R_Date("Beta-627341", 5580, 30);
   R_Date("Beta-627337", 5570, 30);
   R_Date("Beta-627336", 5550, 30);
   R_Date("Beta-627335", 5550, 30);
   R_Date("CSIC-246", 5400, 80);
   Interval("3");
  };
  Boundary("End 3")
  {
   color="red";
  };
  Difference("Difference Phase 1 to Phase 2", "End 1", "Start 2");
  Difference("Difference Phase 2 to Phase 3", "End 2", "Start 3");
 };
};
```

1.3. Charcoal outlier analyses

1.3.1. Single phase charcoal outlier model

Plot()

```
{
 Sequence("Los Murciélagos")
 {
  Boundary("Start Los Murciélagos")
  {
   color="green";
  };
  Phase("Los Murciélagos")
  {
   R_Date("Beta-628426", 8400, 30);
   R_Date("Beta-627332", 8350, 30);
   R_Date("Beta-627333", 8320, 30);
   R_Date("Beta-627334", 8300, 30);
   R_Date("CSIC-247", 7440, 100);
   R_Date("Beta-627342", 6210, 30);
   R_Date("Beta-627340", 6170, 30);
   R_Date("Beta-628427", 6150, 30);
   R_Date("CSIC-1133", 6086, 45);
   R_Date("CSIC-1134", 5900, 38);
   R_Date("CSIC-1132", 5861, 48);
   R_Date("Beta-627338", 5660, 30);
   R_Date("Beta-627331", 5640, 30);
   R_Date("Beta-627330", 5630, 30);
   R_Date("Beta-627341", 5580, 30);
   R_Date("Beta-627337", 5570, 30);
   R_Date("Beta-627336", 5550, 30);
   R_Date("Beta-627335", 5550, 30);
   R_Date("CSIC-246", 5400, 80);
   Interval ("Los Murciélagos");
  };
  Boundary("End Los Murciélagos")
  {
   color="red";
  };
 };
};
```

1.3.2. Two phases charcoal outlier model

```
Plot()
 {
  Outlier_Model("Charcoal",Exp(1,-10,0),U(0,3),"t");
  Sequence("Los Murciélagos")
  {
   Boundary("Start 1")
```

```
{
 color="green";
};
Phase("1")
{
 R_Date("Beta-628426", 8400, 30);
 R_Date("Beta-627332", 8350, 30);
 R_Date("Beta-627333", 8320, 30);
 R_Date("Beta-627334", 8300, 30);
 Interval("1");
};
Boundary("End 1")
{
 color="red";
};
Boundary("Start 2")
{
 color="green";
};
Phase("2")
{
 R_Date("Beta-627342", 6210, 30);
 R_Date("Beta-627340", 6170, 30)
 {
  Outlier("Charcoal",0.05);
 };
 R_Date("Beta-628427", 6150, 30);
 R_Date("CSIC-1133", 6086, 45);
 R_Date("CSIC-1134", 5900, 38);
 R_Date("CSIC-1132", 5861, 48);
 R_Date("Beta-627338", 5660, 30)
 {
  Outlier("Charcoal",0.05);
 };
 R_Date("Beta-627331", 5640, 30);
 R_Date("Beta-627330", 5630, 30);
 R_Date("Beta-627341", 5580, 30);
 R_Date("Beta-627337", 5570, 30);
 R_Date("Beta-627336", 5550, 30);
 R_Date("Beta-627335", 5550, 30);
 R_Date("CSIC-246", 5400, 80);
 Interval("2");
};
Boundary("End 2")
{
 color="red";
```

```
  };
  Difference("Difference Phase 1 to Phase 2", "End 1", "Start 2");
 };
};
```

1.3.3. Three phases charcoal outlier model

```
Plot()
 {
  Outlier_Model("Charcoal",Exp(1,-10,0),U(0,3),"t");
  Sequence("Los Murciélagos")
  {
   Boundary("Start 1")
   {
    color="green";
   };
   Phase("1")
   {
    R_Date("Beta-628426", 8400, 30);
    R_Date("Beta-627332", 8350, 30);
    R_Date("Beta-627333", 8320, 30);
    R_Date("Beta-627334", 8300, 30);
    Interval("1");
   };
   Boundary("End 1")
   {
    color="red";
   };
   Boundary("Start 2")
   {
    color="green";
   };
   Phase("2")
   {
    R_Date("CSIC-247", 7440, 100)
    {
     Outlier("Charcoal",0.05);
    };
    Interval("2");
   };
   Boundary("End 2")
   {
    color="red";
   };
   Boundary("Start 3")
   {
```

```
  color="green";
 };
 Phase("3")
 {
  R_Date("Beta-627342", 6210, 30);
  R_Date("Beta-627340", 6170, 30)
  {
   Outlier("Charcoal",0.05);
  };
  R_Date("Beta-628427", 6150, 30);
  R_Date("CSIC-1133", 6086, 45);
  R_Date("CSIC-1134", 5900, 38);
  R_Date("CSIC-1132", 5861, 48);
  R_Date("Beta-627338", 5660, 30)
  {
   Outlier("Charcoal",0.05);
  };
  R_Date("Beta-627331", 5640, 30);
  R_Date("Beta-627330", 5630, 30);
  R_Date("Beta-627341", 5580, 30);
  R_Date("Beta-627337", 5570, 30);
  R_Date("Beta-627336", 5550, 30);
  R_Date("Beta-627335", 5550, 30);
  R_Date("CSIC-246", 5400, 80);
  Interval("3");
 };
 Boundary("End 3")
 {
  color="red";
 };
 Difference("Difference Phase 1 to Phase 2", "End 1", "Start 2");
 Difference("Difference Phase 2 to Phase 3", "End 2", "Start 3");
};
};
```

Supplementary Figures

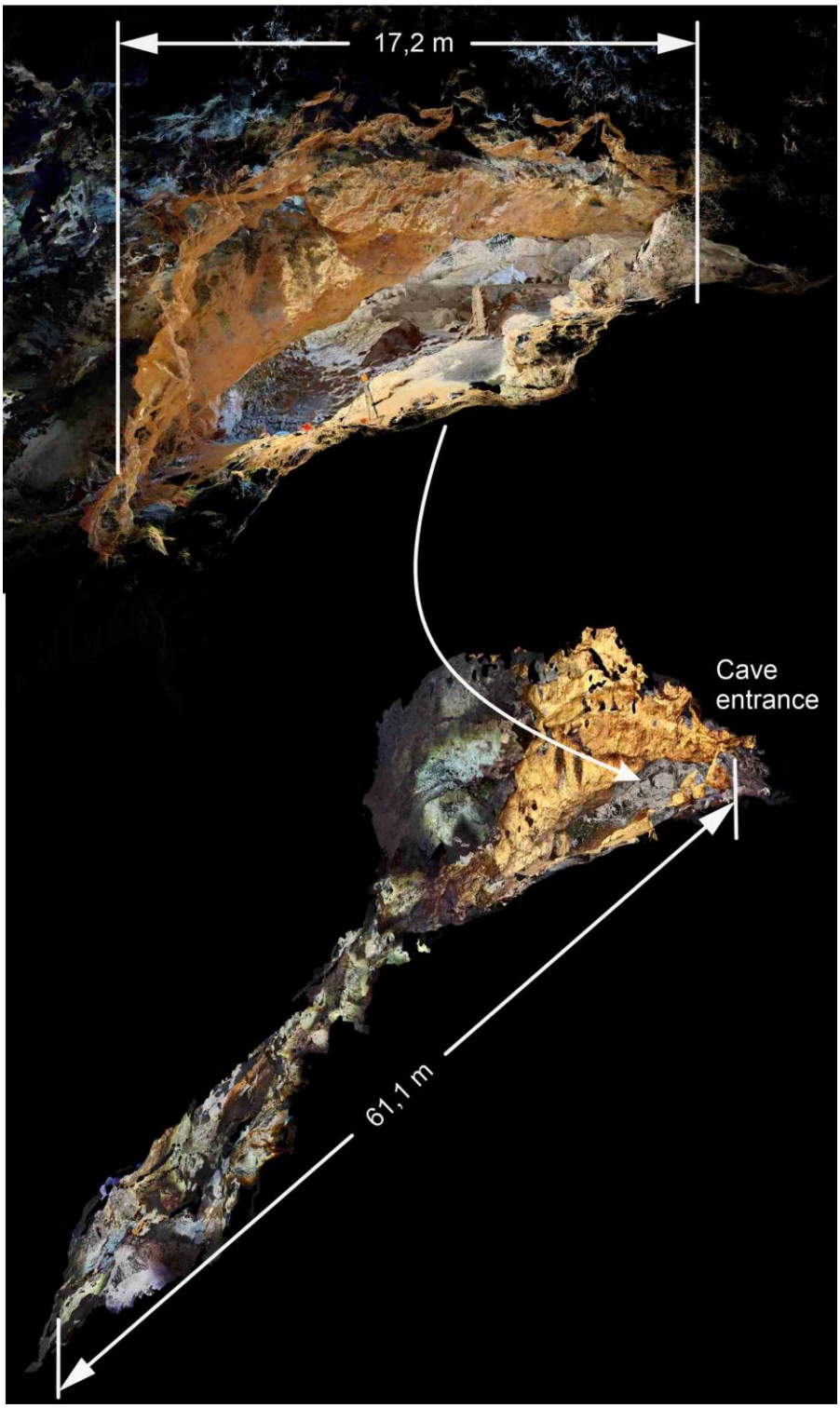

Fig. S1. Cave 3D model with the entrance and cross-section.

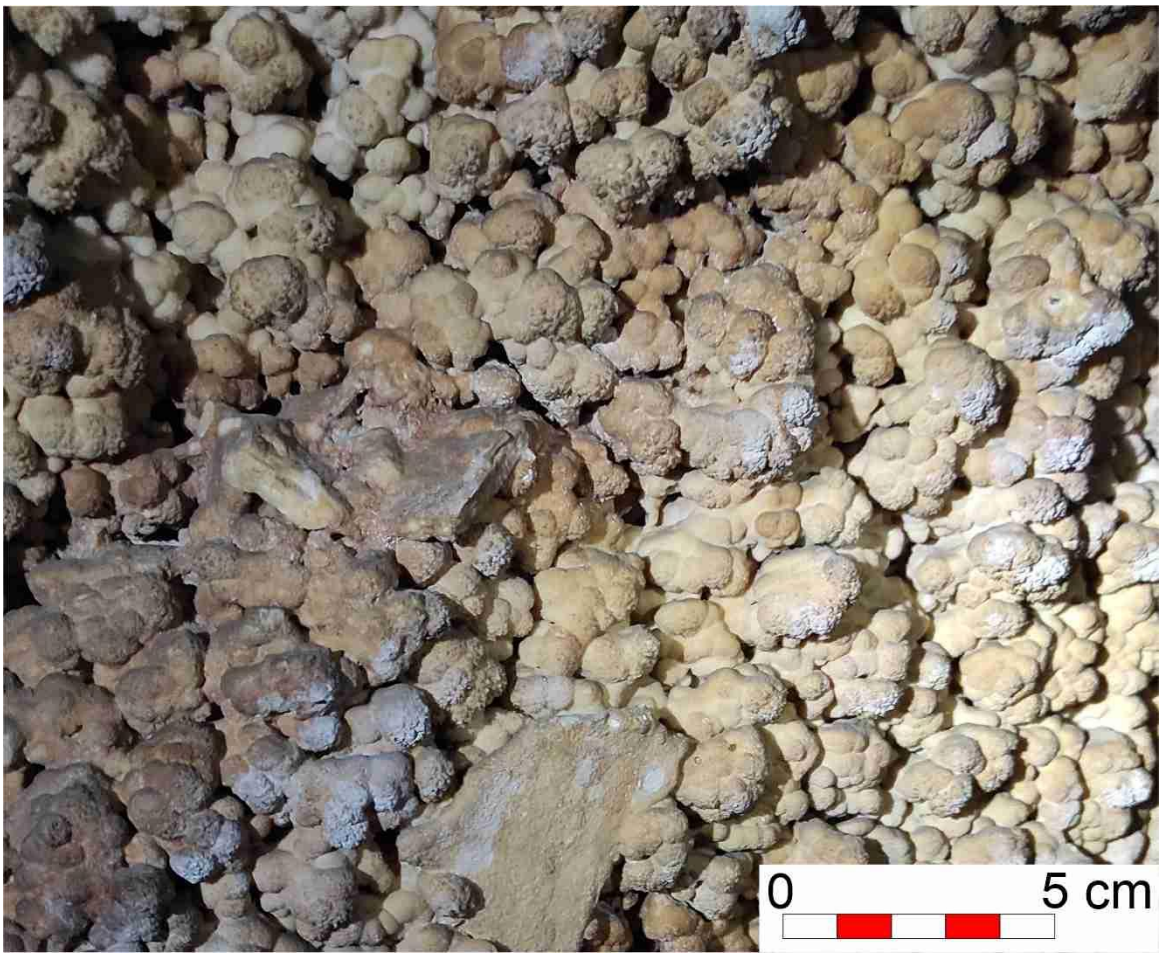

Fig. S2. Detail of globular speleothems in the interior of the cave.

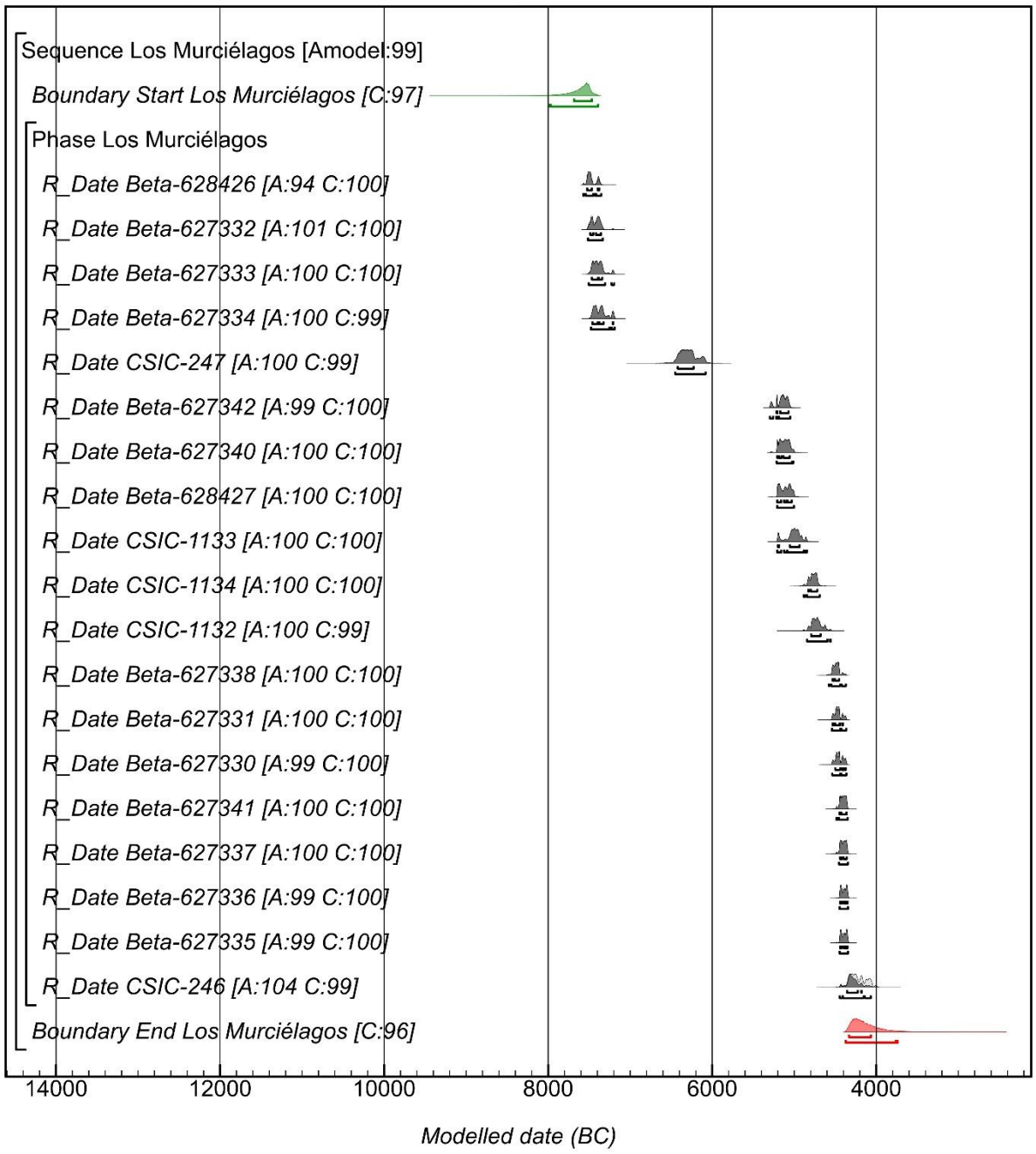

Fig. S3. Single phase Bayesian chronological ranges for the estimated start and end of Cueva de los Murciélagos. The plot also includes the probability distribution of dates. OxCal v4.4.4 Bronk Ramsey (69); r:5 Atmospheric data from Reimer et al. (68).

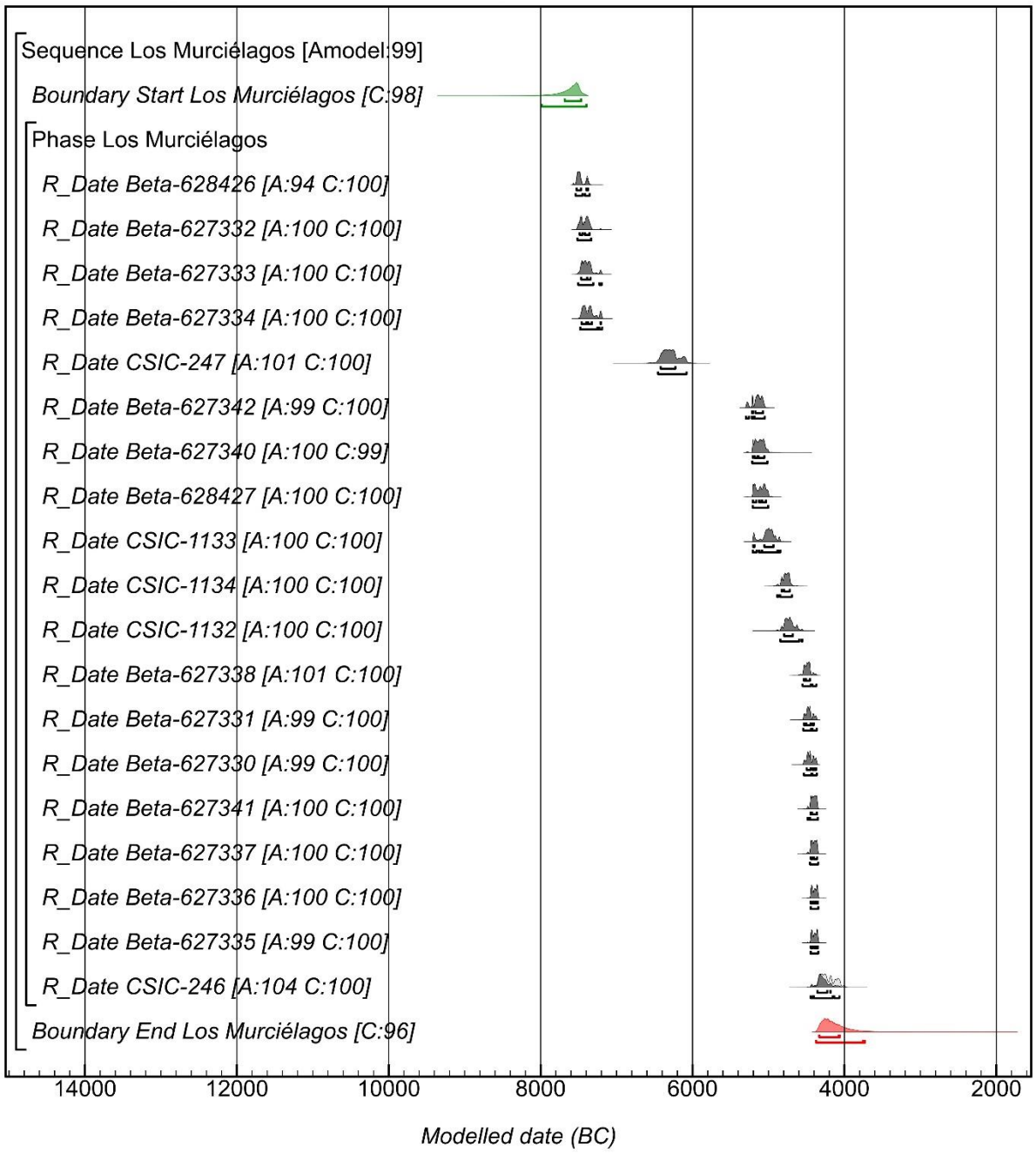

Fig. S4. Bayesian chronological ranges using a Charcoal Outlier single phase model to estimate start and end of each phase of Cueva de los Murciélagos. The plot also includes the probability distribution of dates. OxCal v4.4.4 Bronk Ramsey (69); r:5 Atmospheric data from Reimer et al. (68).

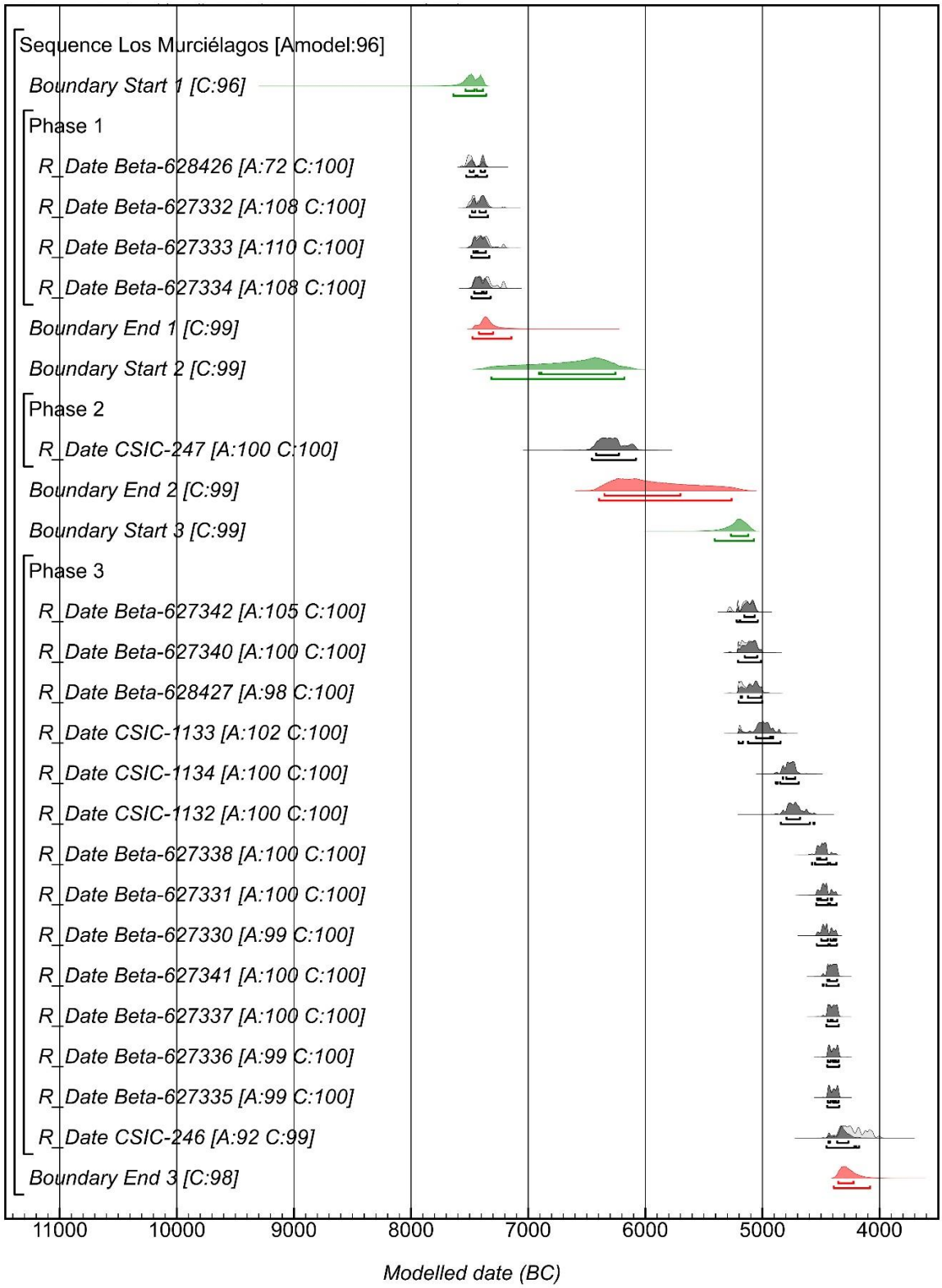

Fig. S5. Multi-phase Bayesian chronological ranges for the estimated start and end of each phase of Cueva de los Murciélagos. The plot also includes the probability distribution of dates. OxCal v4.4.4 Bronk Ramsey (69); r:5 Atmospheric data from Reimer et al. (68).

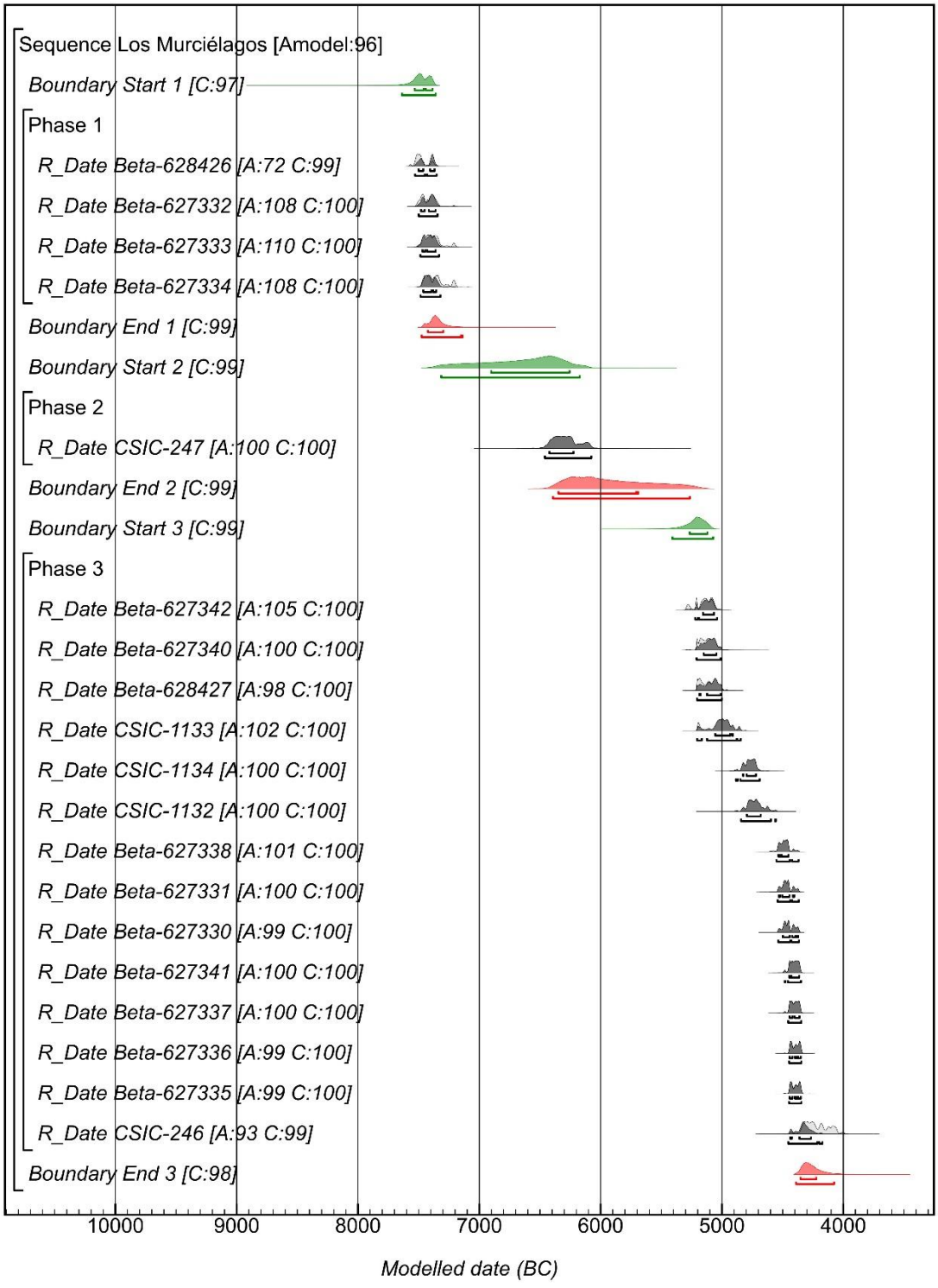

Fig. S6. Bayesian chronological ranges using a Charcoal Outlier multi-phase model to estimate start and end of each phase of Cueva de los Murciélagos. The plot also includes the probability distribution of dates. OxCal v4.4.4 Bronk Ramsey (69); r:5 Atmospheric data from Reimer et al. (68).

Supplementary Tables

Table S1. Plants-based objects inventory from Cueva de los Murciélagos (Albuñol, Granada) (*Museum: MAN Museo Arqueológico Nacional; MAEG Museo Arqueológico y Etnográfico de Granada).

ID	Integrity	Object type	Typology	Material	Raw material identification	Raw material processing	Raw material measurements	Museum*	Others
472	Complete	Spoon	-	Wood	Non-identified	-	-	MAN	
473	Fragmented	Perforated item	-	Wood	*Olea europaea*	-	-	MAN	
474	Fragmented	Bowl	-	Wood	*Erica arborea/australis*	-	-	MAN	
475	Complete	Mallet	-	Wood	*Olea europaea*	-	-	MAN	
476	Complete	Handle	-	Wood	*Evergreen Quercus*	-	-	MAN	
479	Complete	Pointed object	-	Wood	*Arbutus unedo*	-	-	MAN	
579	Complete	3D basket	Simple twined	Vegetal fibers	*Stipa tenacissima*	Raw	1.162	MAN	
580	Almost complete	3D basket	Simple twined	Vegetal fibers	*Stipa tenacissima*	Raw	0.999	MAN	
581	Complete	3D basket	Simple twined	Vegetal fibers	*Stipa tenacissima*	Raw	0.801	MAN	
582	Complete	3D basket	Simple twined	Vegetal fibers	*Stipa tenacissima*	Raw	0.790	MAN	
583	Almost complete	3D basket	Simple twined	Vegetal fibers	*Stipa tenacissima*	Raw	1.050	MAN	
584	Fragmented	3D basket	Simple twined	Vegetal fibers	*Stipa tenacissima*	Raw	0.956	MAN	
585	Complete	3D basket	Simple twined	Vegetal fibers	*Stipa tenacissima*	Raw	1.008	MAN	
586	Almost complete	3D basket	Simple twined	Vegetal fibers	*Stipa tenacissima*	Raw	1.123	MAEG	
586a	Fragmented	Cord	Braided	Vegetal fibers	*Stipa tenacissima*	Raw	1.030	MAN	Possible handle of the 583 basket.
586b	Fragmented	Twisted fibres	Twined	Vegetal fibers	*Stipa tenacissima*	Raw	1.080	MAN	Possible weft fragment of the 583 basket.
587	Fragmented	3D basket	Coiled	Vegetal fibers	*Stipa tenacissima*	Raw and crushed	1.294	MAEG	
588	Fragmented	2D basket	Coiled	Vegetal fibers	*Stipa tenacissima*	Raw and crushed	1.456	MAN	
589	Fragmented	2D basket	Coiled	Vegetal fibers	*Stipa tenacissima*	Raw and crushed	1.263	MAN	
590	Almost complete	3D basket	Coiled	Vegetal fibers	*Stipa tenacissima*	Raw and crushed	1.361	MAN	
591a	Fragmented	Cord	Braided	Vegetal fibers	*Stipa tenacissima*	Crushed	-	MAN	
591b	Fragmented	Cord	Twisted	Vegetal fibers	*Stipa tenacissima*	Crushed	-	MAN	
591c	Fragmented	Cord	Braided	Vegetal fibers	*Stipa tenacissima*	Raw	1.161	MAN	
591d	Fragmented	Cord	Braided and knotted	Vegetal fibers	*Stipa tenacissima*	Crushed	-	MAN	Possible cord from a sandal. Knotted on both ends.
592	Complete	3D basket	Simple twined	Vegetal fibers	*No sampled*	Raw	0.915	MAN	

593	Fragmented	3D basket	Diagonal twined	Vegetal fibers	*Stipa tenacissima*	Raw	0.931	MAEG	
594	Almost complete	3D basket	Pseudobraided/*Cofín*	Vegetal fibers	*Stipa tenacissima*	Raw	1.258	MAN	
595	Complete	Sandal	Central core	Vegetal fibers	*Stipa tenacissima*	Crushed	-	MAN	
596	Complete	Sandal	Central core	Vegetal fibers	*Stipa tenacissima*	Crushed	-	MAN	
597	Complete	Sandal	Central core	Vegetal fibers	*Stipa tenacissima*	Crushed	-	MAEG	
598	Fragmented	Sandal	Central core	Vegetal fibers	*Stipa tenacissima*	Crushed	-	MAN	
599	Almost complete	Sandal	Central core	Vegetal fibers	*Stipa tenacissima*	Crushed	-	MAEG	
600	Fragmented	Sandal	Central core	Vegetal fibers	*Stipa tenacissima*	Crushed	-	MAN	
601	Fragmented	Sandal	Central core	Vegetal fibers	*Stipa tenacissima*	Crushed	-	MAN	
602	Fragmented	Sandal	Central core	Vegetal fibers	*Stipa tenacissima*	Crushed	-	MAN	
603	Almost complete	Sandal	Central core	Vegetal fibers	*Stipa tenacissima*	Crushed	-	MAN	
604	Fragmented	Sandal	Central core	Vegetal fibers	*Stipa tenacissima*	Crushed	-	MAN	
605	Almost complete	Sandal	Central core	Vegetal fibers	*Stipa tenacissima*	Crushed	-	MAN	
606	Complete	Sandal	Central core	Vegetal fibers	*Stipa tenacissima*	Crushed	-	MAN	
607a	Fragmented	Sandal	Central core	Vegetal fibers	*Stipa tenacissima*	Crushed	-	MAN	607a and 607b could be part of the same object.
607b	Fragmented	Sandal	Central core	Vegetal fibers	*Stipa tenacissima*	Crushed	-	MAN	607a and 607b could be part of the same object.
608	Fragmented	Sandal	Central core	Vegetal fibers	*Stipa tenacissima*	Crushed	-	MAN	
609	Fragmented	Sandal	Central core	Vegetal fibers	*Stipa tenacissima*	Crushed	-	MAN	
610	Almost complete	Sandal	Simple	Vegetal fibers	*Stipa tenacissima*	Crushed	-	MAN	
611	Fragmented	Sandal	Simple	Vegetal fibers	*Stipa tenacissima*	Crushed	-	MAN	
612	Almost complete	Sandal	Central core	Vegetal fibers	*Stipa tenacissima*	Crushed	-	MAN	
613	Fragmented	Sandal	Central core	Vegetal fibers	*Stipa tenacissima*	Crushed	-	MAN	
614	Fragmented	Sandal	Central core	Vegetal fibers	*Stipa tenacissima*	Crushed	-	MAN	
615	Fragmented	2D basket	Coiled	Vegetal fibers	*Stipa tenacissima*	Raw and crushed	1.299	MAN	
616a	Fragmented	2D basket	Coiled	Vegetal fibers	*Stipa tenacissima*	Crushed	-	MAN	616a and 616b could be part of the same object.
616b	Fragmented	2D basket	Coiled	Vegetal fibers	*Stipa tenacissima*	Crushed	-	MAN	616a and 616b could be part of the same object.
617	Fragmented	2D basket	Diagonal twined	Vegetal fibers	*Stipa tenacissima*	Raw	1.080	MAN	617, 622, 627, 627a and 627b could be part of the same object.
618	Fragmented	2D basket	Pseudobraided/*Cofín*	Vegetal fibers	*Stipa tenacissima*	Raw	0.745	MAEG	
619	Fragmented	2D basket	Pseudobraided/*Cofín*	Vegetal fibers	*Stipa tenacissima*	Raw	1.224	MAN	
620	Fragmented	2D basket	Coiled	Vegetal fibers	*Stipa tenacissima*	Raw	1.493	MAEG	
621	Fragmented	2D basket	Pseudobraided/*Cofín*	Vegetal fibres	*Stipa tenacissima*	Raw	1.026	MAN	

622	Fragmented	2D basket	Diagonal twined	Vegetal fibres	*Stipa tenacissima*	Raw	1.695	MAEG	617, 622, 627, 627a and 627b could be part of the same object.
623	Fragmented	2D basket	Pseudobraided/*Cofín* distributing warp	Vegetal fibres	*Stipa tenacissima*	Crushed	-	MAN	
624	Fragmented	2D basket	Pseudobraided/*Cofín*	Vegetal fibres	*Stipa tenacissima*	Raw	0.988	MAN	
625	Complete	3D basket	Braided	Vegetal fibres	*Stipa tenacissima*	Raw	1.513	MAN	
626	Complete	Rings	Linked rings	Vegetal fibres	*Stipa tenacissima*	Raw	1.038	MAN	
627	Fragmented	2D basket	Diagonal twined	Vegetal fibres	*Stipa tenacissima*	Raw	1.365	MAEG	617, 622, 627, 627a and 627b could be part of the same object.
627a	Fragmented	2D basket	Diagonal twined	Vegetal fibres	*Stipa tenacissima*	Raw	1.556	MAN	617, 622, 627, 627a and 627b could be part of the same object.
627b	Fragmented	2D basket	Diagonal twined	Vegetal fibres	*Stipa tenacissima*	Raw	1.398	MAN	617, 622, 627, 627a and 627b could be part of the same object.
627c	Fragmented	2D basket	Coiled	Vegetal fibres	*Stipa tenacissima*	Crushed	-	MAN	
627d	Fragmented	2D basket	Coiled	Vegetal fibres	*Stipa tenacissima*	Crushed	-	MAN	
627e	Fragmented	2D basket	Coiled	Vegetal fibres	*Stipa tenacissima*	Crushed	-	MAN	
627f	Fragmented	2D basket	Diagonal twined	Vegetal fibres	*Stipa tenacissima*	Raw	1.363	MAN	
1140	Fragmented	Arrow shaft	-	Wood	*Olea europaea*	-	-	MAEG	
1141	Fragmented	Arrow shaft	-	Wood	*Acer* sp.	-	-	MAN	
1165	Fragmented	Bowl	-	Wood	*Evergreen Quercus*	-	-	MAEG	
1138/532	Fragmented	Arrow shaft	-	Wood, reed and vegetal fibres	*Salix* sp. + *Phragmites* sp. + *Stipa tenacisima*	-	-	MAN	
1139/532	Fragmented	Arrow shaft	-	Reed and vegetal fibres	*Phragmites* sp. + *Stipa tenacisima*	-	-	MAN	
75/82/133	Complete	Cord	Braided and knotted	Vegetal fibres	*Stipa tenacissima*	Crushed	-	MAN	
MUTERMUR-1	Fragmented	Sandal	Central core	Vegetal fibres	*Stipa tenacissima*	Crushed	-	MAN	It had no inventory number in the museum.
MUTERMUR-2	Fragmented	Cord	Knotted fibres	Vegetal fibres	*Stipa tenacissima*	Crushed	-	MAN	It had no inventory number in the museum.

Table S2. Posterior density estimates of multi-phase Bayesian and KDE plots of Cueva de los Murciélagos.

	Unmodelled (BCE/AD)			Modelled (BCE/AD)			Indices Amodel 98.8 Aoverall 99				
	from	to	%	from	to	%	Acomb	A	L	P	C
Start Cueva de los Murciélagos				-7928	-7361	95.4					98.6
KDE_Plot Cueva de los Murciélagos											100
N Cueva de los Murciélagos_Kernel	-2	2	95.4	-2	2.01	95.4		100			99.9
U Cueva de los Murciélagos_Scale	9,97466E-13	1	95.4	62	523	95.4		100			99.8
R_Date Beta-627332	-7516	-7336	95.4	-7512	-7331	95.4		100.2			99.8
R_Date Beta-627333	-7507	-7196	95.4	-7499	-7195	95.4		99.8			99.8
R_Date Beta-627334	-7480	-7192	95.4	-7476	-7192	95.4		99.2			99.8
R_Date CSIC-247	-6455	-6081	95.4	-6454	-6081	95.4		100			99.6
R_Date Beta-627342	-5297	-5050	95.4	-5297	-5050	95.4		99.4			99.9
R_Date Beta-627340	-5214	-5015	95.4	-5214	-5015	95.4		99.7			99.9
R_Date Beta-628427	-5209	-5005	95.4	-5209	-5005	95.4		99.7			99.8
R_Date CSIC-1133	-5208	-4847	95.4	-5208	-4846	95.4		99.8			99.8
R_Date CSIC-1134	-4886	-4690	95.4	-4886	-4690	95.4		99.8			99.8
R_Date CSIC-1132	-4843	-4555	95.4	-4843	-4556	95.4		100			99.6
R_Date Beta-627338	-4581	-4369	95.4	-4552	-4370	95.4		99.8			99.8
R_Date Beta-627331	-4542	-4367	95.4	-4542	-4367	95.4		99.8			99.9
R_Date Beta-627330	-4537	-4365	95.4	-4537	-4365	95.4		99.2			99.9
R_Date Beta-627341	-4486	-4350	95.4	-4484	-4350	95.4		99.7			99.9
R_Date Beta-627337	-4454	-4348	95.4	-4454	-4348	95.4		99.7			99.9
R_Date Beta-627336	-4447	-4346	95.4	-4447	-4346	95.4		99.4			99.9
R_Date Beta-627335	-4447	-4346	95.4	-4447	-4346	95.4		99.4			99.9
R_Date CSIC-246	-4440	-3996	95.4	-4446	-4070	95.4		103.8			99.8
R_Date CSIC-247	-6455	-6081	95.4	-6456	-6082	95.4		100.1			99.7
End Cueva de los Murciélagos				-4377	-3751	95.4					98.3
Start Phase 1				-7687	-7359	95.4					96
KDE_Plot Phase 1											99.5
N Phase 1_Kernel	-2	2	95.4	-2.03	1.98	95.4		100.2			99.3
U Phase 1_Scale	9,97466E-13	1	95.4	416	1	95.4		100			99.2
R_Date Beta-628426	-7576	-7357	95.4	-7531	-7356	95.4		74.9			99.3
R_Date Beta-627332	-7516	-7336	95.4	-7503	-7347	95.4		107.9			99.6
R_Date Beta-627333	-7507	-7196	95.4	-7487	-7336	95.4		109.3			99.4
R_Date Beta-627334	-7480	-7192	95.4	-7485	-7325	95.4		107.6			99.3
End Phase 1				-7480	-7153	95.4					96.1

Start Phase 2				-5384	-5069	95.4		96.1
KDE_Plot Phase 2								100
N Phase 2_Kernel	-2	2	95.4	-2	2.01	95.4	100	99.4
U Phase 2_Scale	9,97466E-13	1	95.4	0.2	0.96	95.4	100	99.2
R_Date Beta-627342	-5297	-5050	95.4	-5220	-5042	95.4	104.5	99.3
R_Date Beta-627340	-5214	-5015	95.4	-5208	-5011	95.4	99.7	99.5
R_Date Beta-628427	-5209	-5005	95.4	-5203	-5001	95.4	97.8	99.5
R_Date CSIC-1133	-5208	-4847	95.4	-5205	-4846	95.4	102.2	99.4
R_Date CSIC-1134	-4886	-4690	95.4	-4887	-4691	95.4	99.7	99.2
R_Date CSIC-1132	-4843	-4555	95.4	-4843	-4555	95.4	99.8	98.8
R_Date Beta-627338	-4581	-4369	95.4	-4552	-4370	95.4	99.8	99.6
R_Date Beta-627331	-4542	-4367	95.4	-4542	-4368	95.4	99.6	99.6
R_Date Beta-627330	-4537	-4365	95.4	-4537	-4365	95.4	99.5	99.6
R_Date Beta-627341	-4486	-4350	95.4	-4485	-4350	95.4	99.8	99.6
R_Date Beta-627337	-4454	-4348	95.4	-4454	-4349	95.4	99.9	99.7
R_Date Beta-627336	-4447	-4346	95.4	-4447	-4346	95.4	99.4	99.6
R_Date Beta-627335	-4447	-4346	95.4	-4447	-4346	95.4	99.4	99.6
R_Date CSIC-246	-4440	-3996	95.4	-4451	-4171	95.4	95.2	98.9
End Phase 2				-4387	-4048	95.4		95.9

Table S3. Posterior density estimates of the single-phase Bayesian model of Cueva de los Murciélagos.

	Unmodelled (BCE/AD)				Modelled (BCE/AD)				Indices Amodel 98.5 Aoverall 98.4				
	68.3%		95.4%		68.3%		95.4%						
	from	to	from	to	from	to	from	to	Acomb	A	L	P	C
Start Cueva de los Murciélagos					-7685	-7468	-7986	-7391					96.5
R_Date Beta-628426	-7531	-7384	-7576	-7357	-7526	-7379	-7571	-7353		94.2			99.6
R_Date Beta-627332	-7491	-7358	-7516	-7336	-7487	-7357	-7515	-7335		100.5			99.6
R_Date Beta-627333	-7469	-7343	-7507	-7196	-7467	-7343	-7505	-7196		100.2			99.7
R_Date Beta-627334	-7463	-7206	-7480	-7192	-7462	-7207	-7479	-7192		99.8			99.4
R_Date CSIC-247	-6421	-6226	-6455	-6081	-6422	-6226	-6453	-6081		100			99.4
R_Date Beta-627342	-5215	-5072	-5297	-5050	-5215	-5072	-5297	-5051		99.4			99.8
R_Date Beta-627340	-5208	-5054	-5214	-5015	-5207	-5055	-5214	-5014		99.8			99.8
R_Date Beta-628427	-5208	-5033	-5209	-5005	-5207	-5033	-5209	-5005		99.8			99.7
R_Date CSIC-1133	-5201	-4936	-5208	-4847	-5201	-4935	-5209	-4847		100			99.6
R_Date CSIC-1134	-4827	-4720	-4886	-4690	-4827	-4720	-4886	-4691		99.6			99.6
R_Date CSIC-1132	-4795	-4681	-4843	-4555	-4795	-4680	-4843	-4555		99.8			99.4
R_Date Beta-627338	-4536	-4453	-4581	-4369	-4535	-4453	-4578	-4370		99.7			99.6
R_Date Beta-627331	-4533	-4406	-4542	-4367	-4533	-4406	-4542	-4367		99.5			99.7
R_Date Beta-627330	-4498	-4371	-4537	-4365	-4499	-4372	-4537	-4365		99.2			99.6
R_Date Beta-627341	-4446	-4364	-4486	-4350	-4446	-4364	-4485	-4350		99.6			99.8
R_Date Beta-627337	-4443	-4360	-4454	-4348	-4443	-4360	-4454	-4348		99.7			99.8
R_Date Beta-627336	-4443	-4350	-4447	-4346	-4443	-4351	-4447	-4346		99.3			99.8
R_Date Beta-627335	-4443	-4350	-4447	-4346	-4443	-4351	-4447	-4346		99.4			99.8
R_Date CSIC-246	-4342	-4068	-4440	-3996	-4357	-4181	-4445	-4068		103.9			99.4
Interval Cueva de los Murciélagos					3209	3620	3109	4045					97.7
End Cueva de los Murciélagos					-4332	-4065	-4373	-3741					96.3

Table S4. Posterior density estimates of the Charcoal Outlier single phase model of Cueva de los Murciélagos.

	Unmodelled (BCE/AD)						Modelled (BCE/AD)						Indices Amodel 99 Aoverall 99				
	from	to	%	from	to	%	from	to	%	from	to	%	Acomb	A	L	P	C
Outlier_Model Charcoal							-44	3	68.3	-239	3	95.4					99.7
Exp (1,-10,0)	-1.24	-0.05	68.3	-3.19	-0.05	95.4											97
U (0,3)	2,21	3	68.3	2,21	3	95.4	3,6	2247	68.3	3,6	2856	95.4		100			99.7
Start Cueva de los Murciélagos							-7683	-7469	68.3	-7988	-7397	95.4					98.3
R_Date Beta-628426	-7531	-7384	68.3	-7576	-7357	95.4	-7526	-7379	68.3	-7541	-7354	95.4		94.3			99.7
R_Date Beta-627332	-7491	-7358	68.3	-7516	-7336	95.4	-7487	-7357	68.3	-7515	-7334	95.4		100.4			99.7
R_Date Beta-627333	-7469	-7343	68.3	-7507	-7196	95.4	-7466	-7343	68.3	-7506	-7196	95.4		100.2			99.7
R_Date Beta-627334	-7463	-7206	68.3	-7480	-7192	95.4	-7462	-7206	68.3	-7479	-7192	95.4		99.7			99.5
R_Date CSIC-247	-6421	-6226	68.3	-6455	-6081	95.4	-6421	-6225	68.3	-6455	-6080	95.4		100.6		95.6	99.6
R_Date Beta-627342	-5215	-5072	68.3	-5297	-5050	95.4	-5215	-5072	68.3	-5297	-5050	95.4		99.4			99.8
R_Date Beta-627340	-5208	-5054	68.3	-5214	-5015	95.4	-5207	-5054	68.3	-5214	-5015	95.4		100		95.4	98.9
R_Date Beta-628427	-5208	-5033	68.3	-5209	-5005	95.4	-5208	-5034	68.3	-5209	-5005	95.4		99.7			99.8
R_Date CSIC-1133	-5201	-4936	68.3	-5208	-4847	95.4	-5201	-4934	68.3	-5208	-4846	95.4		99.8			99.7
R_Date CSIC-1134	-4827	-4720	68.3	-4886	-4690	95.4	-4827	-4720	68.3	-4886	-4691	95.4		99.9			99.6
R_Date CSIC-1132	-4795	-4681	68.3	-4843	-4555	95.4	-4794	-4681	68.3	-4843	-4556	95.4		100			99.7
R_Date Beta-627338	-4536	-4453	68.3	-4581	-4369	95.4	-4534	-4453	68.3	-4552	-4370	95.4		100.8		96	99.6
R_Date Beta-627331	-4533	-4406	68.3	-4542	-4367	95.4	-4532	-4406	68.3	-4542	-4367	95.4		99.4			99.7
R_Date Beta-627330	-4498	-4371	68.3	-4537	-4365	95.4	-4499	-4371	68.3	-4537	-4365	95.4		99.1			99.6
R_Date Beta-627341	-4446	-4364	68.3	-4486	-4350	95.4	-4446	-4364	68.3	-4484	-4350	95.4		99.7			99.9
R_Date Beta-627337	-4443	-4360	68.3	-4454	-4348	95.4	-4443	-4360	68.3	-4454	-4348	95.4		99.7			99.7
R_Date Beta-627336	-4443	-4350	68.3	-4447	-4346	95.4	-4443	-4351	68.3	-4446	-4346	95.4		99.5			99.7
R_Date Beta-627335	-4443	-4350	68.3	-4447	-4346	95.4	-4443	-4351	68.3	-4447	-4346	95.4		99.4			99.7
R_Date CSIC-246	-4342	-4068	68.3	-4440	-3996	95.4	-4357	-4183	68.3	-4445	-4068	95.4		103.9			99.5
Interval Cueva de los Murciélagos							3206	3621	68.3	3109	4055	95.4					97.4
End Cueva de los Murciélagos							-4331	-4063	68.3	-4373	-3734	95.4					95.5

Table S5. Posterior density estimates of the multi-phase Bayesian model of Cueva de los Murciélagos.

	Unmodelled (BCE/AD)			Modelled (BCE/AD)									Indices Amodel 95.8 Aoverall 96.5				
	from	to	%	from	to	%	from	to	%	from	to	%	Acomb	A	L	P	C
Start Phase 1							-7536	-7386	68.3	-7640	-7359	95.4					95.5
R_Date Beta-628426	-7531	-7384	68.3	-7576	-7357	95.4	-7501	-7370	68.3	-7530	-7353	95.4		71.8			99.6
R_Date Beta-627332	-7491	-7358	68.3	-7516	-7336	95.4	-7481	-7361	68.3	-7500	-7345	95.4		107.9			99.6
R_Date Beta-627333	-7469	-7343	68.3	-7507	-7196	95.4	-7469	-7362	68.3	-7486	-7333	95.4		109.6			99.6
R_Date Beta-627334	-7463	-7206	68.3	-7480	-7192	95.4	-7462	-7357	68.3	-7484	-7322	95.4		107.9			99.6
Interval Phase 1							0	170	68.3	0	443	95.4					98.8
End Phase 1							-7422	-7300	68.3	-7476	-7144	95.4					99.1
Start Phase 2							-6907	-6256	68.3	-7315	-6180	95.4					99.3
R_Date CSIC-247	-6421	-6226	68.3	-6455	-6081	95.4	-6421	-6226	68.3	-6456	-6081	95.4		99.7			99.8
Interval Phase 2							5	1003	68.3	0	1647	95.4					99.2
End Phase 2							-6350	-5700	68.3	-6396	-5265	95.4					99.2
Start Phase 3							-5269	-5121	68.3	-5408	-5073	95.4					99.4
R_Date Beta-627342	-5215	-5072	68.3	-5297	-5050	95.4	-5156	-5067	68.3	-5221	-5041	95.4		104.8			99.8
R_Date Beta-627340	-5208	-5054	68.3	-5214	-5015	95.4	-5152	-5045	68.3	-5209	-5013	95.4		100			99.8
R_Date Beta-628427	-5208	-5033	68.3	-5209	-5005	95.4	-5186	-5012	68.3	-5206	-5001	95.4		98.2			99.7
R_Date CSIC-1133	-5201	-4936	68.3	-5208	-4847	95.4	-5055	-4910	68.3	-5205	-4846	95.4		101.8			99.7
R_Date CSIC-1134	-4827	-4720	68.3	-4886	-4690	95.4	-4827	-4720	68.3	-4886	-4690	95.4		100			99.6
R_Date CSIC-1132	-4795	-4681	68.3	-4843	-4555	95.4	-4795	-4680	68.3	-4843	-4556	95.4		99.9			99.6
R_Date Beta-627338	-4536	-4453	68.3	-4581	-4369	95.4	-4535	-4453	68.3	-4579	-4370	95.4		99.9			99.8
R_Date Beta-627331	-4533	-4406	68.3	-4542	-4367	95.4	-4533	-4407	68.3	-4542	-4367	95.4		99.5			99.8
R_Date Beta-627330	-4498	-4371	68.3	-4537	-4365	95.4	-4499	-4371	68.3	-4537	-4365	95.4		99.4			99.8
R_Date Beta-627341	-4446	-4364	68.3	-4486	-4350	95.4	-4446	-4364	68.3	-4485	-4350	95.4		99.8			99.9
R_Date Beta-627337	-4443	-4360	68.3	-4454	-4348	95.4	-4444	-4361	68.3	-4454	-4348	95.4		99.9			99.9
R_Date Beta-627336	-4443	-4350	68.3	-4447	-4346	95.4	-4443	-4351	68.3	-4447	-4346	95.4		99.3			99.7
R_Date Beta-627335	-4443	-4350	68.3	-4447	-4346	95.4	-4443	-4351	68.3	-4447	-4346	95.4		99.4			99.8
R_Date CSIC-246	-4342	-4068	68.3	-4440	-3996	95.4	-4439	-4267	68.3	-4453	-4176	95.4		92.3			99.2
Interval Phase 3							813	1035	68.3	744	1232	95.4					99.3
End Phase 3							-4354	-4223	68.3	-4392	-4082	95.4					98
Difference Phase 1 to Phase 2							-1097	-418	68.3	-1140	-5	95.4					99.3
Difference Phase 2 to Phase 3							-1126	-444	68.3	-1174	-30	95.4					99.3